

PAPER REF: 7125

FATIGUE RESPONSE OF AS BUILT DMLS PROCESSED MARAGING STEEL AND EFFECTS OF MACHINING AND HEAT AND SURFACE TREATMENTS

Dario Croccolo¹, Massimiliano De Agostinis¹, Stefano Fini¹, Giorgio Olmi^{1(*)}, Francesco Robusto¹, Snezana Ciric-Kostic², Aleksandar Vranic², Nusret Muharemovic³, Nebojsa Bogojevic²

¹Department of Industrial Engineering (DIN), University of Bologna, Bologna, Italy

²Faculty of Mechanical and Civil Engineering in Kraljevo, University of Kragujevac, Serbia

³Plamingo d.o.o., Gračanica, Bosnia and Herzegovina

(*)Email: giorgio.olmi@unibo.it

ABSTRACT

The main motivations for this study arise from the need for an assessment of the fatigue performance of DMLS produced Maraging Steel MS1, when it is used in the “as fabricated” state. The literature indicates a lack of knowledge from this point of view, moreover the great potentials of the additive process may be more and more incremented, if an easier and cheaper procedure could be used after the building stage. The topic has been tackled experimentally, investigating the impact of heat treatment, machining and micro-shot-peening on the fatigue strength with respect to the “as built state”. The results indicate that heat treatment significantly enhances the fatigue response, probably due to the relaxation of the post-process tensile residual stresses. Machining can also be effective, but it must be followed (not preceded) by micro-shot-peening, to benefit from the compressive residual stress state generated by the latter.

Keywords: DMLS, Maraging Steel, “as built” state, machining, heat treatment.

INTRODUCTION

The Additive Manufacturing (AM) process is based on layer manufacturing, without any additional tools or machining processes (Bourell, 2009; Aliakbari, 2012; Pandey, 2010; Herderick, 2011) Direct Metal Laser Sintering (DMLS) and Selective Laser Melting are the two most important Additive Manufacturing technologies. Both of them are powder bed-based technologies.

Concept of layered built parts dates from more than one century. AM enables manufacturing without tools, using just one AM machine fed by a CAD model. This is split into two-dimensional layers with constant thickness, by specific software, the layers can be regarded as areas that will be melted with proper thickness. Every new layer is fused with the previous one during the AM process. The part is progressively built, repeating this process until the last layer is stacked.

There are several AM technologies, depending on the handled material, on how the material is applied or fused, etc. Powder Bed technology is based on material application on the entire building surface; afterwards, the laser or electron beam melts the area that corresponds to the sliced surface. The process is repeated, until part completion. Wire or powder feed technology is based on the step-by-step material application and melting, until the surface that corresponds to the sliced layer is formed. In this case, the material is applied to the surface that is being manufactured only. A further classification of the AM techniques deals with the principle of

material melting (laser beam, electro beam, electro-arc etc.). In almost all the technologies for AM of metal parts, the material is completely melted and bonding between layers is achieved during solidification. DMLS and SLM are nowadays quite close technologies and their different names mostly arise from different trademarks (Shellabear, 2004; Nicoletto, 2018). At the early stages of development of these technologies, components after manufacturing were remarkably porous, as not full density could be achieved, due to partial fusion. The smelting and sintering processes were different and the processed materials were mainly based on Iron, Copper and Nickel alloy. Moreover, additional processing was mandatory, to achieve better density and fusion (Campanelli, 2010; Naiju, 2011).

AM technologies are and more and more used in the industrial field and is also attracting interest with regard to biomechanics. Using 3D CT scanners, it is possible to model custom implants that perfectly fit the person's need (Parthasarathy, 2011; Jardini, 2016; Jardini, 2014). Materials with good bio-compatibility can be processed by AM, which gives them good potentials for dental and medical purposes (Bertol, 2010).

The layer based manufacturing provides a particular microstructure affecting the build parts that is different the casted structure of the same wrought material. In AM, material melting and cooling rates are very high. Fast melting is the result of high energy concentration, whereas fast cooling arises from the small amount of melted material with low surrounding temperature. This high temperature gradient usually induces high tensile residual stresses. Part building starts on thick steel plate (base-plate). Part can be built directly on the plate or with an additional support structure, generated between the plate and the part. Its purpose is part constraining, moreover it facilitates heat flow from the part during the scanning (melting) process. The support structure needs to be strong enough, to efficiently restrain any kind of deformation that residual stress can cause. The generation of a residual stress state affecting the fabricated component is indeed a drawback of this process that is usually tackled by suitable heat of surface treatments. Machine manufacturers usually provide some data regarding the mechanical properties of AM built parts in the material datasheets (<https://www.eos.info/material-m>). However, these mainly deal with static properties, such as ultimate tensile strength, yield strength, hardness, mechanical characteristics after ageing etc. Therefore, there is a great interest towards the fatigue response and the impact of the post manufacture treatments.

Maraging steel is one of the most promising materials, for use in Additive Manufacturing (Brookes, 2016). Density of AM built parts are generally higher than 90%. Hardness of AM built parts from Maraging Steel is similar to those made by conventional ways like casting. It has good mechanical properties and it can be a good candidate for high-carbon steel substitution. It is resistant to corrosion and crack initiation during tempering and has good machinability (Yasa, 2010; Kempen, 2011; Casalino, 2015). It has a relatively high ultimate tensile strength (UTS) after the heat treatment, around 2000MPa. Thanks to its high UTS, it is a promising material to be used for structures operating under high states of load in many fields. This becomes more attractive, considering that AM technologies gives the chance to build multi-part object as a single part (https://www.eos.info/industries_markets/aerospace/engines), making it possible to built monolithic complexly shaped components in small batches. Research contributions on the Fatigue limit (FL) and the fatigue strength (FS) of Maraging steel made by some of AM processes are quite limited, to the best of the authors' knowledge. This paper presents a follow-up of a previous research by the same authors (Crocco, 2016).

Components produced by AM can have different orientation with respect to the stacking direction of the layers. The aim of the previous research was to explore the effect of build orientation on the fatigue strength of Maraging Steel samples built by DMLS EOS M280

machine. The obtained results indicate that part orientation did not have significant effect on FS and FL, when the part were treated by micro-shot peening and heat treatment after the stacking process, thus meeting the powder producer recommendations. The components had than been machined with 0.5 mm allowance, in order to get an optimal surface finishing. The aforementioned outcomes were also confirmed by the study (Croccolo (IRF2018), 2018), involving the same material. A further research (Croccolo, 2018) was then focused on Stainless Steel PH1 and led to a partial confirmation: some effect was observed in this case, probably due to different material properties and stacking parameters.

Literature studies dealing with the effects of the stacking process on the mechanical properties of the parts made by AM are few. Most the research deals with the effects of the process parameters as well as of post-processing on tensile static strength (Casati, 2016; Gibson, 1997; Baufeld, 2010). Few papers are concerned with the fatigue strength of Aluminium alloy (Edwards, 2014; Bača, 2016; Konečná, 2016), Inconel alloy (Smith, 2016) and Titanium alloy samples (Brandl, 2012). Review papers have been written, trying to collect all the technologies and all the available mechanical testing results (Lewandowski, 2016). However, a lack of consistency between the testing procedures and the obtained results can be noticed, when all these data are merged together.

There is nowadays an increasing interest in lowering down post-manufacturing expenses in AM, and in speeding up the process from design to installation. Sometimes, post processing is not possible, for instance, when treating lattice structures, cooling channels in injection moulds or in turbine blades. In particular, machining or shot-peening cannot be performed on internal surfaces, on the other hand, running an heat treatment could be expensive and time consuming. This interest is also testified by some recent studies (Nicoletto, 2018; Kahlin, 2017) that have dealt with the fatigue properties of Ti-6Al-4V in its as built state. It is clear that the as built surface condition is likely to introduce a detrimental effect on fatigue with respect to the machined condition. Therefore, an intensive study is needed to clarify if post-processing treatments, including machining or heat treatment, can be skipped and, if so, how the best compromise between costs and the strength that can be accomplished. This was the main motivation that led to this study, whose aim was to investigate the effects of heat treatment, machining and shot-peening on the fatigue response of DMLS built Maraging Steel. This topic has been tackled experimentally: for this purpose, an experimental campaign has been arranged as a factorial plane, with a total amount of five treatment combinations. Fatigue tests have been run on all the sample types, finally working out the fatigue curves in the finite life domain and the fatigue limits. These results have then been compared and discussed, based on statistical methods.

MATERIALS AND METHODS

The testing procedure was based on ISO 1143 Standard for rotating bending fatigue testing (ISO 1143, 2010). The Standard defines the testing procedure, the load scheme and the specimen geometry. Specimens were designed with cylindrical smooth geometry with uniform 6mm diameter at the gage. The smallest recommended dimension by the Standard has been chosen as the best compromise, between Standard consistency and manufacturing costs. A drawing of the specimen is shown in Fig. 1. The specification regarding surface quality was not considered for the “as built”, to properly account for the influence of machining.

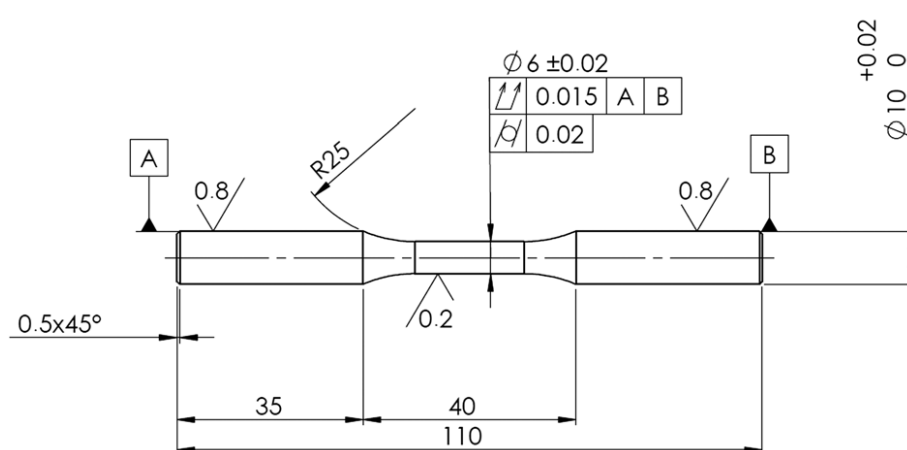


Fig.1 Technical drawing of the sample for fatigue tests under rotating bending (all dimensions in mm)

The specimens have been manufactured by M280 DMLS machine (EOS GmbH – Electro Optical Systems, Germany), equipped by Ytterbium fibre laser with 200W power and emitting 0.2032mm thickness and 1064nm wavelength infrared light beam (https://www.eos.info/systems_solutions/metal/systems_equipment/eosint_m280). Specimen material was MS1 maraging steel MS1 (by EOS GmbH – Electro Optical Systems, Germany), equivalent to 1.2709 steel (https://www.eos.info/material_m/werkstoffe/download/EOS_MaragingSteel_MS1.pdf) and also reported as 18% Ni Maraging 300 or AISI 18Ni300. The chemical composition of the material is provided in Table 1. Specimen manufacturing was done in the processing chamber of the machine with working area of 250×250mm in horizontal plane and with maximum building height up to 325mm. The base plate was preheated to the temperature of 40°C.

Table 1 Chemical composition of Maraging steel MS1

Ni [%]	Co [%]	Mo [%]	Ti [%]	Al [%]	Cr [%]	Cu [%]	C [%]	Mn [%]	Si [%]	P [%]	S [%]	Fe [%]
17-19	8.5-9.5	4.5-5.2	0.6-0.8	0.05-0.15	≤ 0.5	≤ 0.5	≤ 0.03	≤ 0.1	≤ 0.1	≤ 0.01	≤ 0.01	Bal.

Manufacturing process typically takes place in nitrogen inert atmosphere, generated from compressed air by nitrogen generator that is built inside machine. The process chamber consists of three platforms and recoater: The Dispenser platform, where material powder is contained, the Building platform, on which the base plate is set and the building process is done, the Collector platform for the collection of excess material. A scheme of the building chamber is shown in Fig. 2.

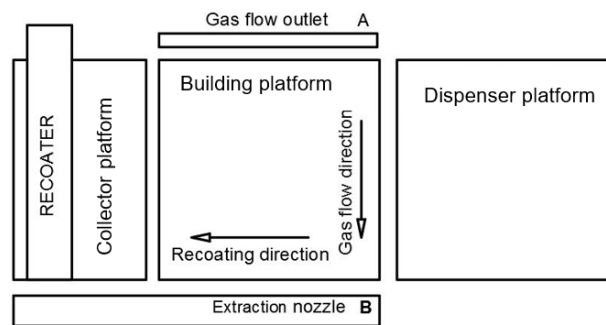


Fig.2 A scheme of the chamber of the utilised EOS machine

The material was applied with $40\mu\text{m}$ thickness that corresponds to the recommended layer thickness for the MS1 Maraging Steel. The building parameters (laser speed, laser power, laser offset, layer thickness etc.) of the EOSINT M280 for MS1 sample manufacturing were kept constant for all the stacking tasks. They were provided by the EOS as a predetermined set of parameters named “PERFORMANCE”. This parameter set can be regarded as a good compromise between surface quality and manufacturing speed.

The canning strategy consisted in parallel traces on every layer; for next layer, scanning strategy was rotated by an angle of 67° . The contour of the scanned surface was finally rescanned, in order to get better surface quality. Example of the scanning process is shown in Fig. 3 a).

The specimens were built directly on the base plate, with vertical orientation, without using a support structure, Fig. 3 c). Proceeding this way, the surface quality of the specimens in the as fabricated state was unaffected by the support structure teeth traces on the surface. After the building process, the specimens were taken from the process chamber, cleaned from excessive powder by micro-shot-peening, using stainless steel spherical shots with $400\mu\text{m}$ diameter under a flow pressure of 5 bar. This treatment is usually performed, to close the process induced porosities and to generate compressive residual stresses that slightly reduce the tensile residual state induced upon fabrication. The samples were then cut off from the base plate, by wire cutting with Electrical Discharge Machining (EDM).



Fig.3 a) As Built specimens during scanning, b) Specimens cleaning from powder, c) Specimens after micro-shot-peening

The samples planned for heat treatment underwent age-hardening by heating in oven. The temperature was increased from room temperature to 490 °C in 1h, afterwards, they were kept at constant temperature for additional 5h (total 6h process), before gradual cooling in fresh air. This heat treatment is usually recommended, to achieve a reduction of the process induced tensile residual stresses, with a potential beneficial effect on the fatigue response of the built parts (Sanz, 2013; Aboulkhair, 2016). Then, the specimens planned for machining, were ground with 0.5 mm allowance with the aim of achieving the surface quality required by the ISO 1143 Standard as well as to improve the fatigue performance (ISO 1143, 2010).

The experimental campaign was arranged, according to the scheme in Table 2: in particular, the 2-by-2 design was run first, in order to investigate the impacts of heat treatment and machining with surface refinement. The sample set named N involved samples that underwent micro-shot-peening, but neither heat treatment not machining. The samples from set M were micro-shot-peened and then machined, whereas those of set H underwent micro-shot-peening and subsequent aging treatment. Finally, for the HM condition, consisting in peened, heat treated and machined samples, the global curve determined in (Croccolo (IRF2018), 2018) was used. As explained in this reference, it can be regarded as the most general and reliable model for the fatigue behaviour in the full treatment condition at the current state of the art.

Table 2 Design of the experiment

Aging Heat Treatment	Machining			
	No	Yes	Yes, with subsequent shot-peening	Set MP
No	Set N	Set M		
Yes	Set H	Set HM		

The experimental design was then completed by the addition of a further combination, named MP: in this case, the samples underwent machining just after fabrication and then shot-peening by steel shots with 0.7 mm diameter. This surface treatment was carried out with shot flow under 5 bar pressure. This latest combination was added, to investigate the effect of the different post-processing order on the fatigue response. The main motivation supporting this choice was that, despite the material manufacturer recommendations, the beneficial residual stress state yielded by post-fabrication peening was likely to be completely removed by the subsequent machining with 0.5 allowance.



Fig.4 a) Clamped specimen after breakage, b) Specimen running, c) Chuck collet

The specimens were mounted on the testing rig, tightening their heads into chuck collet, on both sides of the specimen Fig. 4. Load was kept constant and bending moment was constant at gage during testing. The Testing rig, for four-point rotating bending was described in (Croccolo, 2016).

The samples were tested until failure or until 10^7 cycles, to be regarded as run-out. Each sample set consisted of 7 to 15 specimens. Using the aforementioned procedure, it was possible to obtain FL and the S-N curve for finite life domain. The fatigue limit was obtained by the Dixon stair-case method for small number of sample trials with failure or non-failure outcomes (Dixon, 1969). The Dixon method is a modified stair-case method that makes it possible to estimate FL even from small series of nominal trials (in this case four to seven). Standard deviation was estimated to estimate the uncertainty and to determine the confidence band for FL at the 90% confidence level. ISO 12107 was used for processing the data in finite life domain (ISO 12107, 2012). Data were linearly interpolated in logarithmic diagram. Upper and lower bounds of the logarithmic curve were determined, based on the standard deviation of fatigue life, with the probability of failure of 90% for upper limit and 10% for lower limit and with the confidence level of 90%.

EXPERIMENTAL PROCEDURE

All the samples have undergone geometry measurement, to check requirements accomplishment. Diameter dimension and surface roughness have been measured at the head and at the gage. For this purpose, a micrometre screw gauge, (with the resolution of 0.01mm) and a portable surface roughness tester (with the resolution of 0.01 μm , Handysurf E-30A; Carl Zeiss AG, Oberkochen, Germany) have been used.

Diameter measurement checks have been done at two points at the heads, replicating measurement with 90° rotations at each point, for a total of eight replications, including both the specimen heads. Diameter at the gauge was measured at three points, with two replications for each, by 90° rotation, for an overall number of 6 replications.

Surface roughness on both heads and on the gage was measured over 8 replications. In particular, roughness was averaged over 4 mm runs along the longitudinal axis, considering 90° angled spots with two repetitions for each. Measurement at the gage was performed only on the samples that got broken during the fatigue testing, due to the impossibility to correctly align the roughness tester in the unbroken ones. The retrieved measurements were anyway sufficient to get evidence of the roughness mean value at gage.

Some average values of the diameter and surface roughness measurements are provided in Table 3 with reference to Set N. Specimen types 1 and M are well consistent with the drawing requirements presented in Fig.1. Surface roughness values for the unmachined specimen types were almost five times higher than specifications, which is reasonable, considering that these specimens were in as-built condition.

Table 3 Dimensional and roughness (Ra) measurements with regard to the samples of Set N

Specimen ID	Gage diameter			Head diameter (left side)			Head diameter (right side)		
	Mean [mm]	St. dev. [mm]	Roughness Ra [μm]	Mean [mm]	St. dev. [mm]	Roughness Ra [μm]	Mean [mm]	St. dev. [mm]	Roughness Ra [μm]
N.1	6.09	0.012	4.24	10.07	0.020	5.54	10.06	0.024	3.92
N.2	6.09	0.010	4.12	10.08	0.004	5.48	10.07	0.004	4.47

N.3	6.08	0.008	3.97	10.06	0.010	5.19	10.05	0.014	4.49
N.4	6.09	0.008	4.37	10.07	0.013	4.74	10.05	0.017	4.53
N.5	6.09	0.005	4.57	10.07	0.019	5.28	10.05	0.015	5.49
N.6	6.09	0.009	---	10.07	0.012	4.75	10.06	0.014	4.68
N.7	6.09	0.010	---	10.08	0.007	4.43	10.06	0.009	4.77
N.8	6.09	0.007	---	10.07	0.008	4.24	10.05	0.018	4.76
N.9	6.09	0.007	4.07	10.06	0.010	4.76	10.05	0.019	4.18
N.10	6.09	0.009	5.12	10.08	0.011	5.65	10.05	0.019	6.02
N.11	6.10	0.012	4.54	10.08	0.014	4.72	10.06	0.018	4.83
N.12	6.08	0.012	2.30	10.07	0.015	4.86	10.05	0.006	4.34
N.13	6.08	0.009	3.75	10.08	0.008	5.10	10.06	0.012	4.57
N.14	6.09	0.014	4.21	10.05	0.003	4.48	10.05	0.018	4.07

The fatigue tests were carried out, loading the samples under four-point rotary bending. Tightening was done in such a way that specimen heads could not have any chance to revolve inside chuck collets. After specimen was mounted, radial misalignment of the gage section was checked, as recommended by the aforementioned Standard. Testing was done under rotating bending load with stress ratio $R=-1$ and with the frequency of 60Hz. Fractographic and micrographic analysis have been done as well for some samples, after the end of the testing campaign to examine fracture initiation and propagation areas. In particular, some specimens were cut, embedded into phenolic resin, and polished for micrographic analysis, as in Fig. 5.



Fig.5 Sample preparation for micrographies, in particular the resin embedded sample (longitudinal and cross sections) is depicted on the right

Specimen surface was etched with combination of 150cc of water (H₂O), 50cc of Chloridric Acid (HCl), 25cc of Nitric Acid (HNO₃) and 1g of Calcium Chloride. Etching was done at room temperature for 70 seconds.

RESULTS

The results of the testing campaign are collected in Tables 4 to 7. The Tables provide data regarding specimen ID, nominal stress value at the gage, observed life and comment regarding the trial outcome. In particular, “Run-out” indicates that the specimen survived testing at given load after 10⁷ cycles, whereas “Y” indicates that failure occurred. In this case, the number of cycles to failure is also reported.

Table 4 Results of the fatigue tests on the samples of Set N

Specimen ID	Stress [MPa]	Life [N]	Failure
N.1	610	175,804	Y
N.2	550	236,637	Y
N.3	490	3,577,212	Y
N.4	430	8,336,653	Y
N.5	400	9,659,056	Y
N.6	370	Run-out	N
N.7	400	Run-out	N
N.8	430	Run-out	N
N.9	460	8,069,582	Y
N.10	430	Run-out	N
N.11	460	9,900,777	Y
N.12	610	151,212	Y
N.13	550	156,691	Y
N.14	490	687,908	Y

Table 5 Results of the fatigue tests on the samples of Set H

Specimen ID	Stress [MPa]	Life [N]	Failure
H.2	579	65,841	Y
H.4	550	73,082	Y
H.7	520	169,324	Y
H.15	490	779,587	Y
H.1	460	Run-out	N
H.3	490	8,503,786	Y
H.5	460	198,385	Y
H.6	460	2,589,275	Y
H.16	430	Run-out	N
H.8	460	2,614,325	Y
H.9	579	100,886	Y
H.10	550	2,245,442	Y
H.17	490	Run-out	N
H.11	520	124,220	Y
H.12	490	131,030	Y
H.13	490	20,111,214	N
H.14	550	640,238	Y

Table 6 Results of the fatigue tests on the samples of Set M

Specimen ID	Stress [MPa]	Life [N]	Failure
M.1	610	81,160	Y
M.2	520	219,333	Y
M.3	460	2,415,186	Y
M.4	400	7,885,879	Y
M.5	370	3,035,027	Y
M.6	340	Run-out	N
M.7	370	7,879,073	Y
M.8	340	Run-out	N
M.9	370	Run-out	N
M.10	400	5,662,050	Y

Table 7 Results of the fatigue tests on the samples of Set MP

Specimen ID	Stress [MPa]	Life [N]	Failure
19.12	400	Run-out	N
19.1	430	7,156,630	Y
19.3	460	7,486,110	Y
19.7	490	3,327,981	Y

19.8	520	1,513,780	Y
19.2	580	1,424,868	Y
19.4	520	2,397,072	Y
19.5	490	1,968,952	Y
19.6	460	5,462,365	Y
19.10	430	5,398,139	Y
19.9	400	Run-out	N
19.11	430	Run-out	N
19.13	460	4,550,671	Y
19.15	820	29,369	Y

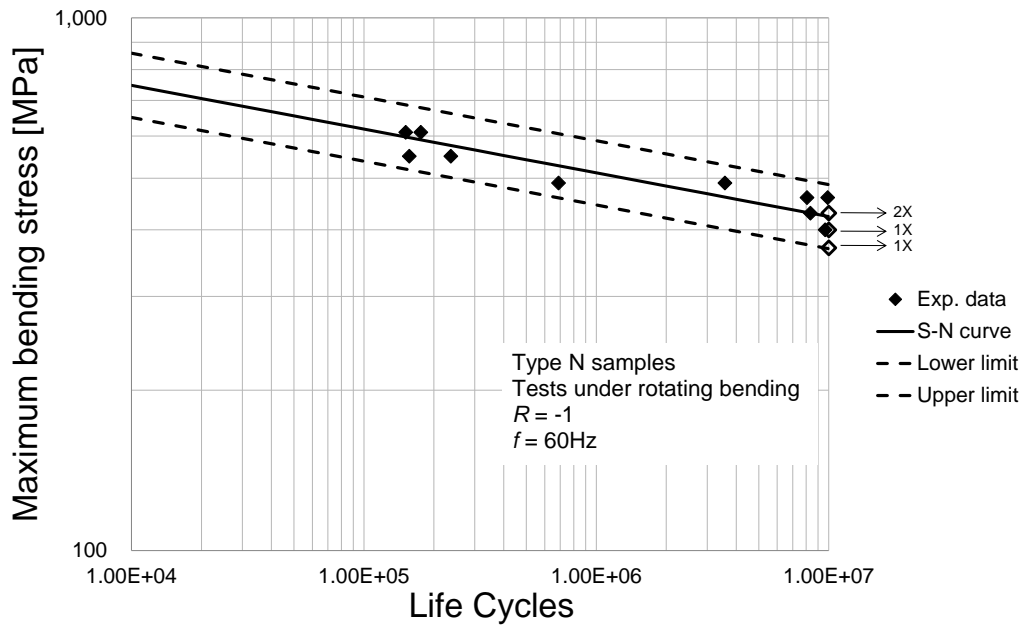


Fig.6 S-N curve along with its confidence band with regard to Set N

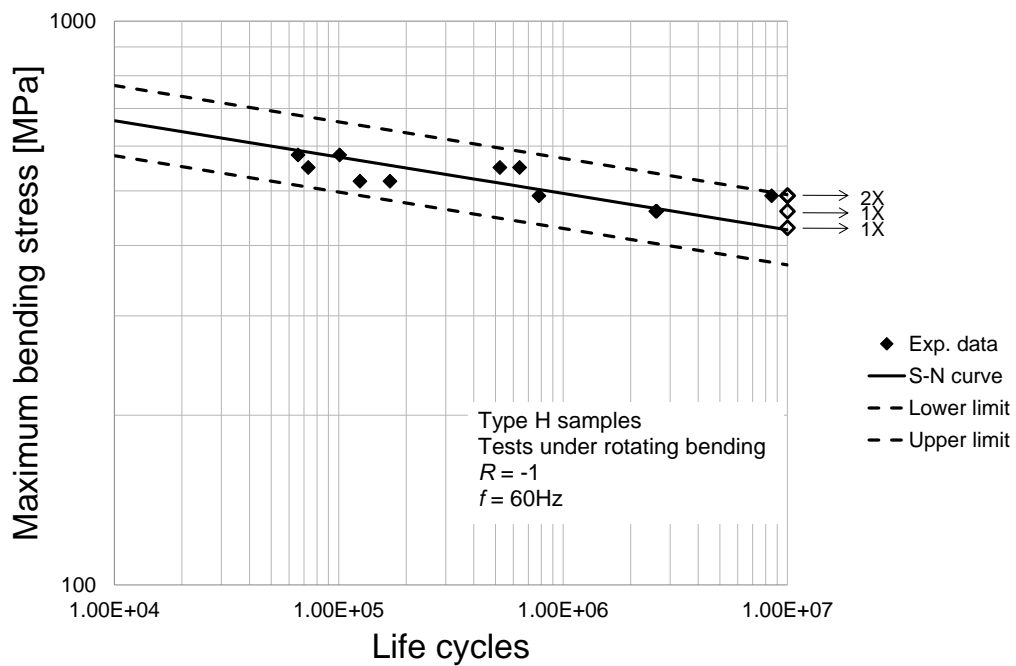


Fig.7 S-N curve along with its confidence band with regard to Set H

The results of the fatigue tests were processed, to obtain the S-N curves in the finite life domain (ISO 12107, 2012). Curves trends together with their upper (90% failure probability) and lower (10% failure probability) bounds at the 90% confidence level, are shown in Figs 6 to 9 (with reference to Sets N, H, M, MP), using double logarithmic scale, including also details regarding specimen type, load ratio and testing frequency, and arrows indicating run outs. The related equations are provided in Table 8, in the terms of the coefficients of the formulas in Eq.s (1) and (2), considering the linear model that proved to be the most suitable, based on (ISO 12107, 2012) .

$$\text{Log}(N) = b_0 + b_1 \cdot \text{Log}(S) \tag{1}$$

$$S = 10^{\frac{b_0}{b_1}} \cdot N^{\frac{1}{b_1}} \tag{2}$$

Table 8 Coefficients of the determined S-N curves, according to the linear model of (ISO, 2012), with reference to Eq.s (1-2)

Set ID	b_0	b_1	$10^{\frac{-b_0}{b_1}}$	$\frac{1}{b_1}$
N	38.99	-12.18	1,592	-0.082
H	47.73	-15.49	1,207	-0.065
M	30.20	-9.06	2,146	-0.110
MP	28.69	-8.26	2,970	-0.121

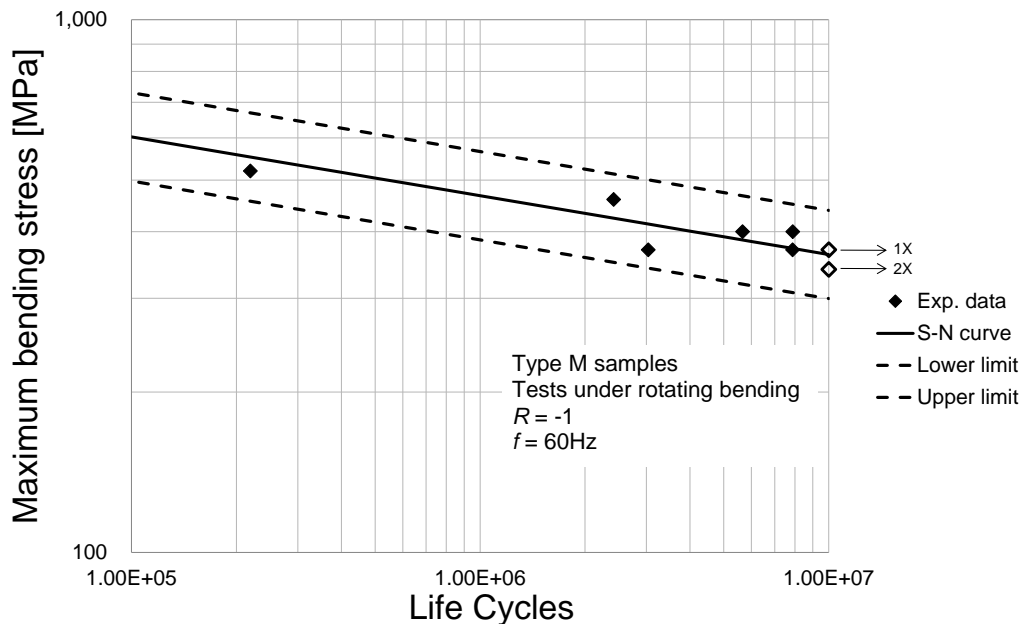


Fig.8 S-N curve along with its confidence band with regard to Set M

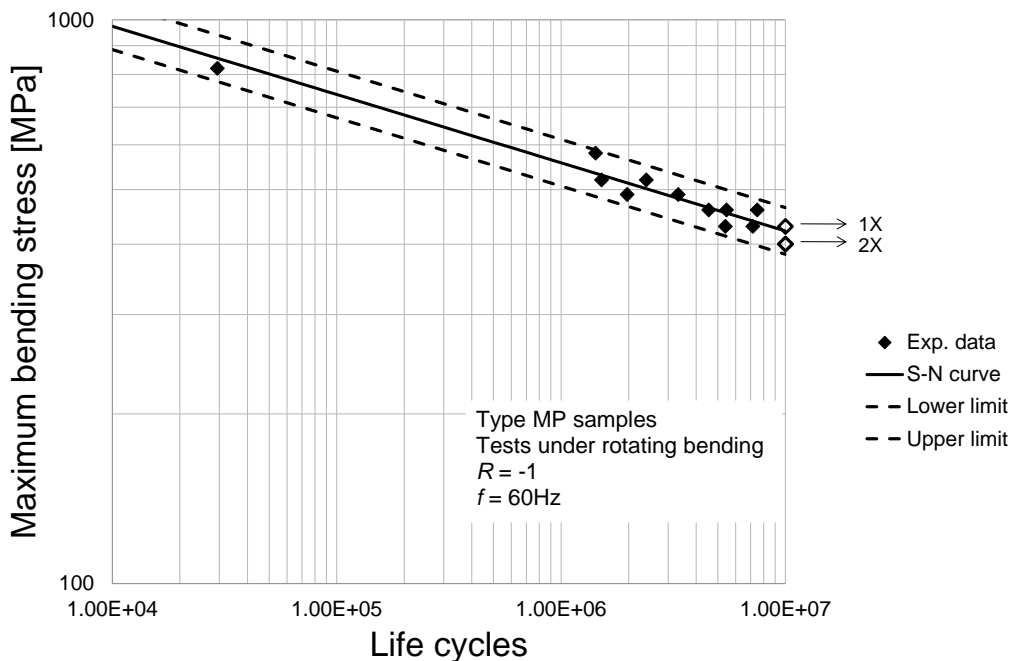


Fig.9 S-N curve along with its confidence band with regard to Set MP

DISCUSSION

The S-N curves in the finite life domain were processed by the ANOVA-based methodology that was introduced in (Olimi, 2012) and successfully applied in (Croccolo, 2016; Croccolo (IRF2018), 2018). The 2-by-2 plane was treated first, following the procedure that is described in more details in (Croccolo, 2016). The Analysis of Variance was followed by the Fisher test, to discuss the significance of the effects of the heat treatment and of machining along with their interaction. The outcome (reported in Table 9), based on a lifespan ranging from 10^4 and 10^7 , was that both factors were highly significant, accepting a probability of error, commonly regarded as p-value, in the order of 10^{-5} . The interaction is also significant with a p-value around 10^{-6} .

Table 9 ANOVA Table for the two-factor design (lifespan between 10^4 and 10^7)

	Sum of squares	Degrees of freedom	Failure	Fisher's ratio	p-value
SSBR: Effect of the heat treatment	0.0164	1	0.0164	19.71	$3 \cdot 10^{-5}$
SSBC: Effect of machining	0.0187	1	0.0187	22.51	10^{-5}
SSI: Interaction	0.0236	1	0.0236	28.39	10^{-6}
SSE: Error	0.0633	76	0.0008		

The four curves, corresponding to the sets referenced as N, M, H, and HM are plotted together in the graph in Fig. 10. It can be observed that, starting from the curve for Set N, coloured in black, the red one for Set H is very close, whereas the yellow one for Set M indicates a slightly lower strength.

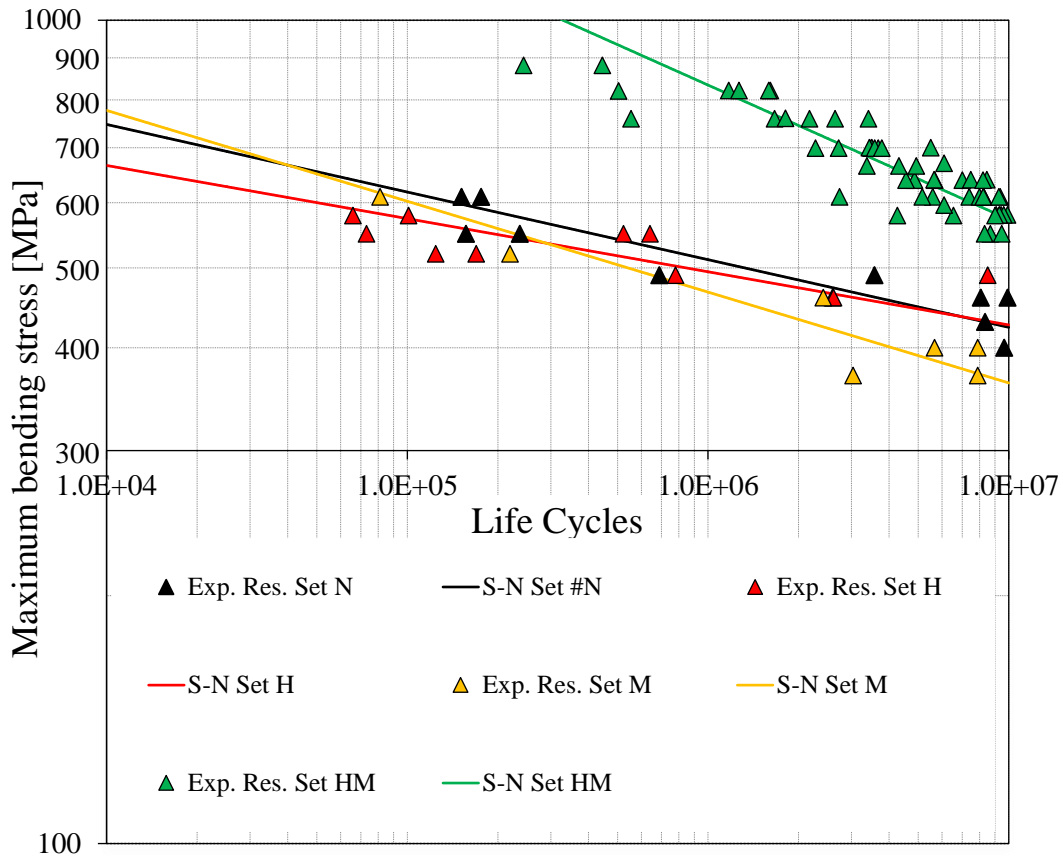


Fig.10 Comparison between the S-N curves in the finite life domain for Sets N, M, H, and HM

These results were interpreted in the light of a further analysis. The same procedure being described in (Croccolo (IRF2018), 2018), regarding one-way ANOVA, was here applied to compare the two curves (black and red) corresponding to the Sets (N and H) in the as built state with and without heat treatment. The same procedure was subsequently applied to compare the S-N plots (black and yellow) for the samples without heat treatment in the as fabricated state or that underwent machining. In both cases, the outcome was the differences are not significant, i.e. the curves are statistically the same. Regarding the effect of heat treatment without machining, it must be remarked that the build process of a Maraging Steel usually leads to a not high tensile residual stress field, due to the low coefficient of thermal expansion (CTE), if compared to that of other materials, e.g. Stainless Steel (Croccolo 2016). In fact, the lower CTE, the lower the induced residual stresses (Fergani, 2017; Croccolo, 2018). Therefore, considering the lower amount of residual stresses, being also reduced by shot-peening, the application of heat treatment becomes ineffective. In other words, the peening treatment seems to provide a sufficient contribution against the process induced not remarkably high tensile residual stresses.

The further outcome of the performed analysis, i.e. the counter-intuitive slightly detrimental effect of machining, can be explained with reference to the beneficial compressive residual stresses induced by micro-shot-peening being removed by machining. This result indicates that the positive effect of surface finishing is compensated by the simultaneous removal of the surficial layers, where the peening induced compressive state was able to provide some protection against crack propagation. This effect can be observed in the not heat treated

samples, where micro-shot-peening plays indeed an important role at relaxing the detrimental tensile residual stresses, as also remarked in the previous paragraph.

Finally, regarding the forth curve, the green one for the HM condition, it keeps much higher than all the others. It indicates the high positive interaction between the two considered factors: in other words, if they are applied together, they have a synergic effect at remarkably enhancing the fatigue strength. On one hand, the heat treatment becomes highly beneficial, when the effect of shot peening is removed through machining, and machining is also significantly beneficial, as it refines the surface, while simultaneously the heat treatment drops down the residual stress state induced by the stacking process.

A final analysis was conducted, including also the curve for the MP Set. The S-N curves for Sets N, M and MP, i.e. for all the Sets, which did not undergo the aging treatment, are plotted together in Fig. 11. The tool of one-way ANOVA with three levels has been utilised again to compare the three curves. The result was that the fatigue strength in the finite life domain is significantly incremented, when shot-peening is performed after machining, i.e. when the curve for the MP Set is compared to the other two ones. This outcome is a further proof for the importance of shot-peening: applying it after machining makes it possible to take advantage of both the induced compressive residual stress (which compensates that induced by the building process, in absence of heat treatment) and the better surface finishing.

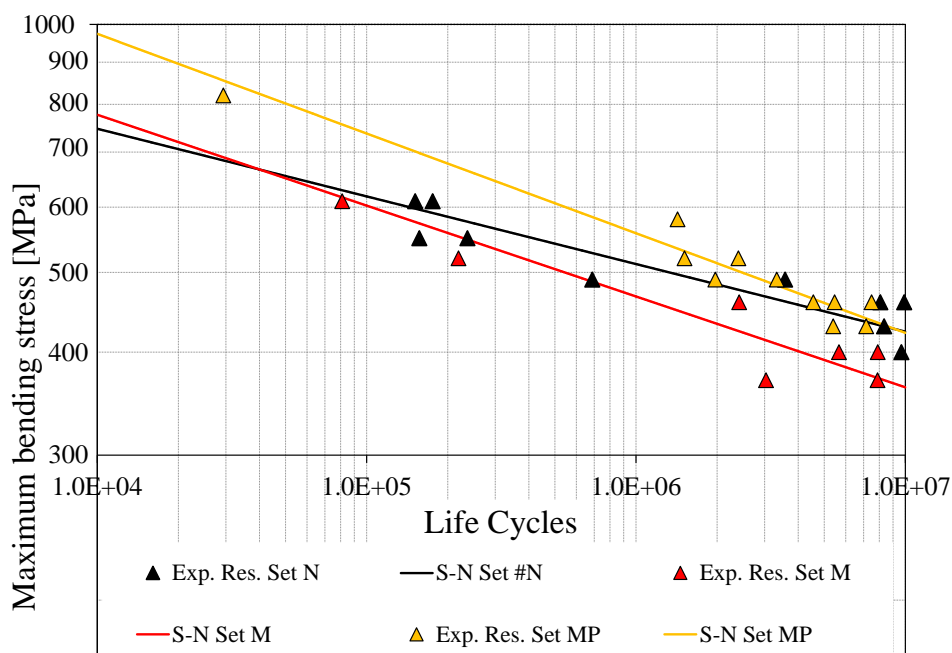


Fig.11 Comparison between the S-N curves in the finite life domain for Sets N, M, and MP

The fatigue limits for all the sample types with their confidence band (90% confidence level) are shown in the bar graph in Fig. 12. As mentioned above, the fatigue limits were worked out by the Dixon method with related confidence analysis, except for Set HM: in this case, the fatigue limit was extrapolated by the S-N curve as the stress corresponding to an expected life of 10^7 cycles. The scatter evaluated in the finite life region was also applied at the fatigue limit, while keeping the same level of confidence for comparison purposes (Meneghetti, 2017). The estimated value of FL for sample type HM is 573MPa, for sample type H is 471MPa, for sample type N is 426MPa, for sample type M is 363MPa, finally for Set MP is 423 MPa. The

sample sets named H and HM underwent heat treatment, whereas the other three ones were without heat treatment. The UTS of MS1 Maraging Steel is 1100MPa in the as built condition, after hardening it is incremented up to 2050MPa, corresponding to almost 100% increase of UTS, following heat treatment (https://www.eos.info/material_m/werkstoffe/download/EOS_MaragingSteel_MS1.pdf).

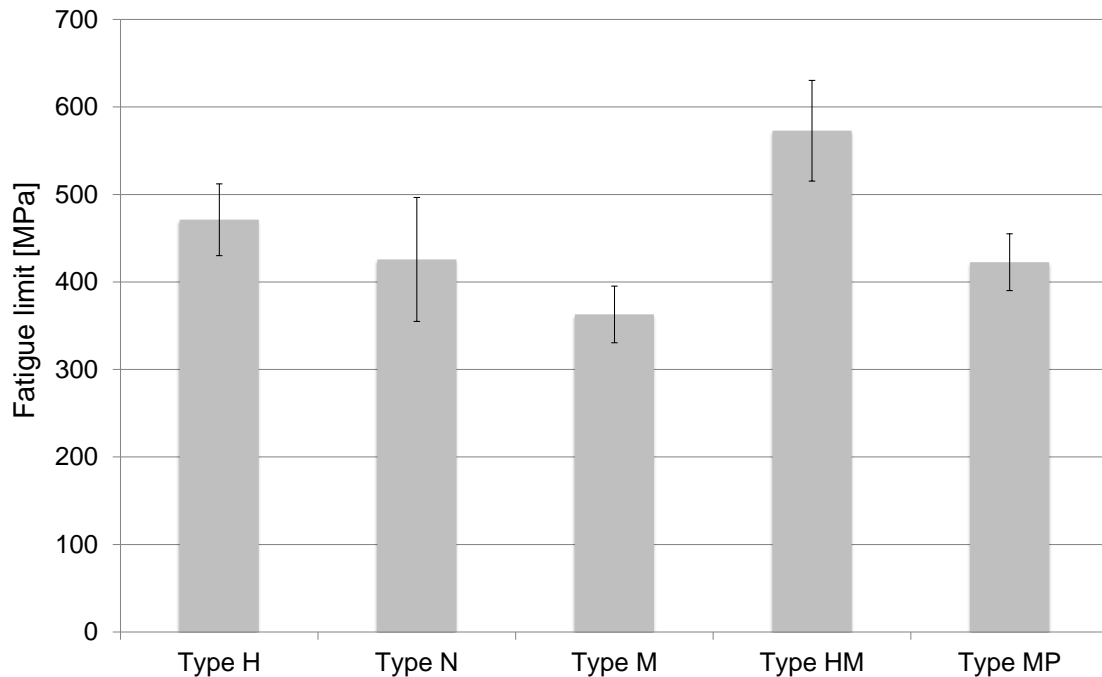


Fig.12 Fatigue limits for 10 million cycle run-out with regard to all the sample Sets in the experimental design.

Regarding Sample types HM and H, their FL is respectively 28% and 23% of UTS. Sample types N, M and MP were without hardening and their FL is indeed lower, but respectively 38%, 33%, 38% of the corresponding UTS without heat treatment. Moreover, the Sets N and MP have very close FLs, whereas the latter yields much better performance for finite life, as remarked above. These ratios are much lower than the commonly accepted ratios of FL over UTS of 50% for machined samples, but are in agreement with some literature research, when considering as built parts (Stoffregen, 2014; Niemann, 2005). This is not surprising, due to the layered characteristic of specimens. Sample type N proved to have a greater FL than machined sample type M.

During fractographic and micrographic analysis some porosities were observed. During fractographic analysis of break surface of both sides of the broken sample, it was found that crack initiation and nucleation starts at one point on the surface or just beneath it, at a distance of about 80 μm from the surface, as shown in Fig. 13. Some amount of voids and inclusions were noticed on fractured surface of all samples. It is indeed possible that voids or inclusions were responsible for crack initiation: most cracks actually seem to start from such defects. Only one crack initiation point was generally observed.

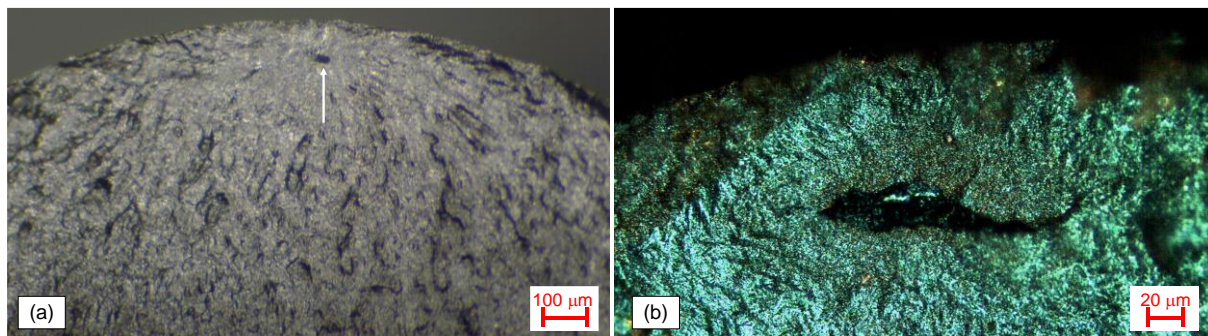


Fig.13 (a) A crack initiating from a porosity in a sample of Set M; (b) a large void that triggered a failure in a specimen of Set H.

It must be pointed out that laser scanning traces were visible both in longitudinal and in transverse sections, regardless of heat treatment execution.

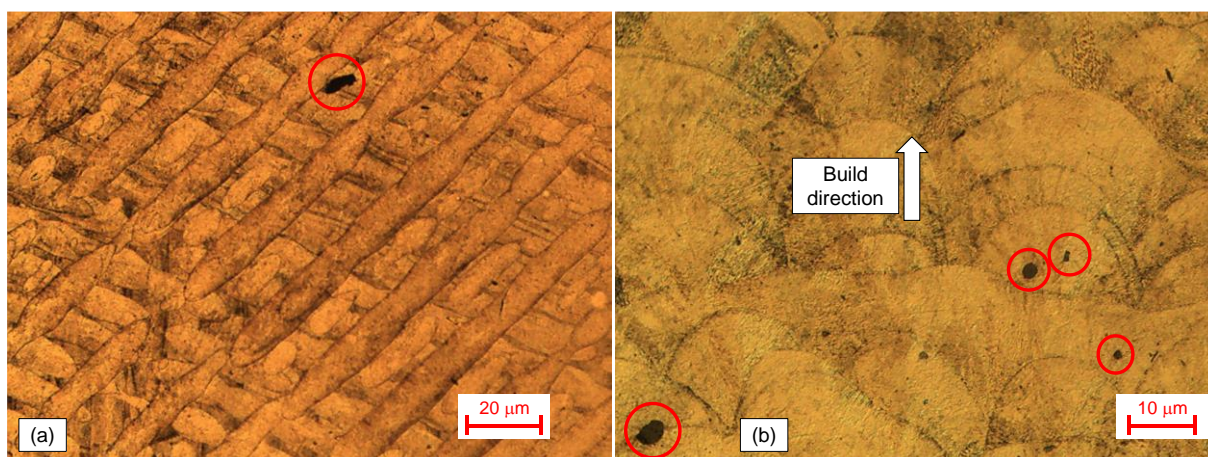


Fig.14 Micrographies on a sample of Set N (without heat treatment) depicting (a) laser scans over the build plane and (b) stacked layers along the build direction. Inclusions are highlighted.

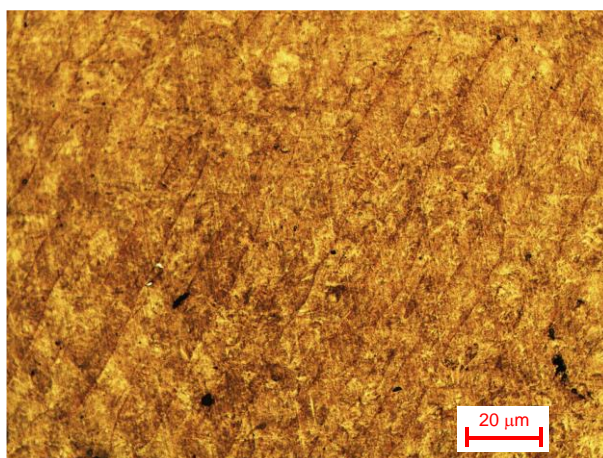


Fig.15 Micrograph on a sample of Set H (with heat treatment), depicting laser scans over the build plane (cross section)

Some inclusions were noticed and marked with arrows in Fig. 14. The scanning pattern in build plane section in Fig.14 (a) indicates some scanning traces underneath with rotation angles corresponding to the aforementioned angle of 67° . Specimens without heat treatment had more pronounced scanning traces than those that had undergone the heat treatment by age hardening, which had conversely a more uniform microstructure. The microstructure of a sample of Set H is shown in Fig. 15. This outcome indicates that heat treatment had some effect on fusion of the laser traces but was not effective at completing deleting these traces. For all the four sample types a comparable amount of inclusion was observed. Heat treatment had no effect on the presence of porosities in material.

CONCLUSIONS

This paper aims at a study on machining and heat treatment effects on fatigue limit and fatigue strength of Maraging Steel specimens manufactured by DMLS EOSINT M280 machine. Five sample sets were considered, all with vertical stacking direction during building. All the four initial sets underwent micro-shot-peening after the building process. One Set was tested in the as built condition, without heat treatment, a second one underwent an aging heat treatment but was kept in the as fabricated state. A third set was machined without heat treatment. Finally, an S-N curve coming from previous studies was used for comparison reason: it refers to samples that underwent heat treatment and then machining, as recommended by the material manufacturer. All the experimental results were processed for the determination of S-N curves in the finite life domain and fatigue limits. Statistical methods were used to compare the curves and their outcomes indicated that heat treatment without machining has a negligible effect, as shot-peening is able to reduce the process induced residual stress state, which is not particularly high due to material properties. The generally positive effect of machining is compensated by the removal of the surface layers treated by micro-shot-peening, when heat treatment is not performed. Finally, when heat treatment and machining are applied together, they have a synergic beneficial effect and the fatigue strength is remarkably incremented.

A fifth set was added to the experiment to investigate, if performing the peening treatment after machining without heat treatment could have a positive effect on the fatigue strength. The statistical analysis confirmed this outcome: refining the surface and then applying a compressive residual stress state leads to a fatigue enhancement in the finite life domain. It is important to remark that a good tuning of the post-process parameters can lead to a fatigue limit in the order of almost 40% the ultimate tensile strength, just ten points lower than the commonly accepted 50% ratio for wrought material.

The study was completed by fractographic and micrographic analyses. The first ones made it possible to individuate some porosities, which were the main sources for crack initiation at approximately $80\ \mu\text{m}$ from the surface. The second one made it possible to compare the microstructures with and without the heat treatment. In the first case, the scanning traces are still visible, but the microstructure is made more uniform.

As a future development of this research, the case of shot peening being performed on heat-treated and machined samples will be considered. Moreover, it will be also the chance to investigate the effect of the position on the chamber on the fatigue response.

ACKNOWLEDGMENTS

The research presented in this paper has received funding from the European Union's Horizon 2020 research and innovation programme under the Marie Skłodowska-Curie grant agreement No. 734455.

REFERENCES

Bourell DL, Beaman JJ, Leu MC, Rosen DW. A brief history of additive manufacturing and the 2009 roadmap for additive manufacturing: looking back and looking ahead. In Proceedings of RapidTech, 2009, p. 24-25.

Aliakbari M. Additive manufacturing: State-of-the-art, capabilities, and sample applications with cost analysis. Master of Science Thesis, Production Engineering and Management, Department of Industrial Production, KTH, Stockholm, Sweden, 2012.

Pandey PM. Rapid prototyping technologies, applications and part deposition planning. Department of Mechanical Engineering Indian Institute of Technology, India, 2010.

Herderick E. Additive manufacturing of metals: A review. *Materials Science & Technology*, 2011, p. 1413-1425.

Shellabear M, Nyrhilä O. DMLS-Development history and state of the art. In Laser Assisted Netshape Engineering 4, Proceedings of the 4th LANE, 2004, p. 21-24.

Nicoletto G. Directional and notch effects on the fatigue behavior of as-built DMLS Ti6Al4V. *International Journal of Fatigue*, 2018, 106, p. 124-131.

Campanelli SL, Contuzzi N, Angelastro A, Ludovico AD. Capabilities and performances of the selective laser melting process. In *New Trends in Technologies: Devices, Computer, Communication and Industrial Systems*. InTech, 2010.

Naiju CD, Adithan M, Radhakrishnan P. An Investigation of Process Variables Influencing Fatigue Properties of Components Produced by Direct Metal Laser Sintering. *KMUTNB: International Journal of Applied Science and Technology*, 2011, 4(1), p. 63-69.

Parthasarathy J, Starly B, Raman S. A design for the additive manufacture of functionally graded porous structures with tailored mechanical properties for biomedical applications. *Journal of Manufacturing Processes*, 2011, 13(2), p.160-170.

Jardini AL, Larosa MA, Macedo MF, Bernardes LF, Lambert CS, Zavaglia CAC, Maciel Filho R, Calderoni DR, Ghizoni E, Kharmandayan P. Improvement in Cranioplasty: Advanced Prosthesis Biomanufacturing. *Procedia CIRP*, 2016, 49, p. 203-208.

Jardini AL, Larosa MA, Maciel Filho R, de Carvalho Zavaglia CA, Bernardes LF, Lambert CS, Calderoni DR, Kharmandayan P. Cranial reconstruction: 3D biomodel and custom-built implant created using additive manufacturing. *Journal of Cranio-Maxillofacial Surgery*, 2014, 42(8), p.1877-1884.

Bertol LS, Júnior WK, da Silva FP, Aumund-Kopp C. Medical design: direct metal laser sintering of Ti-6Al-4V, 2010, *Materials & Design*, 31(8), p.3982-3988.

<https://www.eos.info/material-m>

Brookes KJ. Maraging steel for additive manufacturing – Philipp Stoll's paper at DDMC 2016. *Metal Powder Report*, 2016, 71(3), p.149-152.

Yasa E, Kempen K, Kruth JP, Thijs L, Van Humbeeck J. Microstructure and mechanical properties of maraging steel 300 after selective laser melting. In Solid Freeform Fabrication Symposium Proceedings, 2010, p. 383-396.

Kempen K, Yasa E, Thijs L, Kruth JP, Van Humbeeck J.. Microstructure and mechanical properties of Selective Laser Melted 18Ni-300 steel. Physics Procedia, 2011, 12, p.255-263.

Casalino G, Campanelli SL, Contuzzi N, Ludovico AD. Experimental investigation and statistical optimisation of the selective laser melting process of a maraging steel. Optics & Laser Technology, 2015, 65, p.151-158.

https://www.eos.info/industries_markets/aerospace/engines

Croccolo D, De Agostinis M, Fini S, Olmi G, Vranic A, Ciric-Kostic S. Influence of the build orientation on the fatigue strength of EOS Maraging steel produced by additive metal machine. Fatigue & Fracture of Engineering Materials & Structures, 2016, 39, p. 637-647.

Croccolo D, De Agostinis M, Fini S, Olmi G, Robusto F, Muharemovic N, Bogojevic N, Vranic A, Ciric-Kostic S. Experimental study on the sensitivity of DMLS manufactured Maraging Steel fatigue strength to the build orientation and allowance for machining. In Proceedings of the 6th International Conference INTEGRITY-RELIABILITY-FAILURE (IRF2018), Lisbon, Portugal, 2018.

Croccolo D, De Agostinis M, Fini S, Olmi G, Bogojevic N, Ciric-Kostic S. Effects of build orientation and thickness of allowance on the fatigue behaviour of 15–5 PH stainless steel manufactured by DMLS. Fatigue & Fracture of Engineering Materials & Structures, 2018, 41, p. 900-916.

Casati R, Lemke JN, Tuissi A, Vedani M. Aging Behaviour and Mechanical Performance of 18-Ni 300 Steel Processed by Selective Laser Melting. Metals, 2016, 6(9), 218, p. 1-13

Gibson I, Shi D. Material properties and fabrication parameters in selective laser sintering process. Rapid Prototyping Journal, 1997, 3(4), p.129-136.

Baufeld B, Van der Biest O, Gault R. Additive manufacturing of Ti–6Al–4V components by shaped metal deposition: microstructure and mechanical properties. Materials & Design, 2010, 31, Supplement 1, p. S106-S111.

Edwards P, Ramulu M. Fatigue performance evaluation of selective laser melted Ti–6Al–4V. Materials Science and Engineering: A, 2014, 598, p.327-337.

Bača A, Konečná R, Nicoletto G, Kunz L. Influence of build direction on the fatigue behaviour of Ti6Al4V alloy produced by direct metal laser sintering. Materials Today: Proceedings, 2016, 3(4), p. 921-924.

Konečná R, Kunz L, Bača A, Nicoletto G. Long fatigue crack growth in Ti6Al4V produced by direct metal laser sintering. Procedia Engineering, 2016, 160, p.69-76.

Smith DH, Bicknell J, Jorgensen L, Patterson BM, Cordes NL, Tsukrov I, Knezevic M. Microstructure and mechanical behavior of direct metal laser sintered Inconel alloy 718. Materials Characterization, 2016, 113, p. 1-9.

Brandl E, Heckenberger U, Holzinger V, Buchbinder D. Additive manufactured AlSi10Mg samples using Selective Laser Melting (SLM): Microstructure, high cycle fatigue, and fracture behavior. Materials & Design, 2012, 34, p.159-169.

Lewandowski JJ, Seifi M. Metal additive manufacturing: a review of mechanical properties. Annual Review of Materials Research, 2016, 46, p.151-186.

Kahlin M, Ansell H, Moverare JJ. Fatigue behaviour of additive manufactured Ti6Al4V, with as-built surfaces, exposed to variable amplitude loading. *International Journal of Fatigue* 2017, 103, p. 353-362.

International Organization for Standardization ISO 1143:2010 (E) Metallic Materials – Rotating Bar Bending Fatigue Testing, International Organization for Standardization (ISO), Geneva, Switzerland, 2010.

https://www.eos.info/systems_solutions/metal/systems_equipment/eosint_m280

https://www.eos.info/material_m/werkstoffe/download/EOS_MaragingSteel_MS1.pdf

Sanz C, Navas VG. Structural integrity of direct metal laser sintered parts subjected to thermal and finishing treatments. *Journal of Materials Processing Technology*, 2013, 213(12), p.2126-2136.

Aboulkhair NT, Maskery I, Tuck C, Ashcroft I, Everitt NM. Improving the fatigue behaviour of a selectively laser melted aluminium alloy: Influence of heat treatment and surface quality. *Materials & Design*, 2016, 104, p.174-182.

Dixon WJ, Massey FJ. *Introduction to statistical analysis* (Vol. 344). McGraw-Hill, New York, United States, 1969.

International Organization for Standardization ISO 12107:2012, Metallic Materials – Fatigue Testing – Statistical Planning and Analysis of Data, International Organization for Standardization (ISO), Geneva, Switzerland, 2003.

Olm G. Low cycle fatigue experiments on Turbogenerator steels and a new method for defining confidence bands. *Journal of Testing and Evaluation*, 2012, 40 (4), Paper ID JTE104548.

Fergani O, Berto F, Welo T, Liang SY. Analytical modelling of residual stress in additive manufacturing. *Fatigue & Fracture of Engineering Materials & Structures*, 2017, 40, p. 971-978.

Meneghetti G, Dengo C, Lo Conte F. Bending fatigue design of case-hardened gears based on test specimens. *Proceedings of the Institution of Mechanical Engineers, Part C: Journal of Mechanical Engineering Science*, 2017, DOI: 10.1177/0954406217712278.

Stoffregen HA, Butterweck K, Abele E. Fatigue analysis in selective laser melting: review and investigation of thin-walled actuator housings. In *25th Solid Freeform Fabrication Symposium*, 2014.

Niemann G, Winter H, Hohn BR. *Maschinenelemente*, Springer-Verlag, Berlin, Germany, 2005.